

Supporting Information

Sulfur Confinement via C–S Bonding for Stable Sulfur Conversion in Aqueous Zn–S Batteries

Jiaoyi Ning,^{*‡a} Yunyan Chen,^{‡a} Yunxiang Wen,^a Mingjun Wang,^a Tie Shu,^a Xiao Li,^a Liang Li,^b Yuxing Zhang,^c Ke Xin Yao^{*}

^a School of Chemistry and Chemical Engineering, Multi-Scale Porous Materials Center, Institute of Advanced Interdisciplinary Studies, Chongqing University, No. 174 Shazheng Street, Shapingba District, Chongqing, 400044, China. E-mail: jiaoyi.ning@cqu.edu.cn, kexinyao@cqu.edu.cn

^b Department of Sciences and Engineering, Sorbonne University Abu Dhabi, 38044 Abu Dhabi, United Arab Emirates.

^c School of Materials Science and Engineering, Chongqing University, Chongqing 400044, China.

1. Materials and methods

1.1. Materials

Sublimated sulfur (S), zinc trifluoromethanesulfonate ($\text{Zn}(\text{OTf})_2$, 98%, Macklin), zinc iodide (ZnI_2 , 98.68%, Picasso), ethylene glycol (EG, AR, Keshi), 3,4-dimethoxythiophene ($\geq 97\%$ Aladdin), but-3-en-1-ol ($\geq 98\%$ Aladdin), p-toluenesulfonic acid ($\geq 98.5\%$ Aladdin), toluene ($\text{C}_6\text{H}_5\text{CH}_3$ AR Macklin), anhydrous magnesium sulfate (MgSO_4 AR Aladdin), petroleum ether (PE AR Keshi), dichloromethane (CH_2Cl_2 AR Keshi), polytetrafluoroethylene preparation (PTFE, 60 wt%, aladdin), carbon disulfide ($>99.00\%$, Macklin), Ketjen Black (KB, ECP-600JD, Lion Corporation), Ethyl Alcohol ($\text{C}_2\text{H}_6\text{O}$, AR, Keshi), Zn foil (80 μm), glass fiber (GF/D, 0.68 mm, Whatman). The chemicals used in the process are analytically pure.

1.2. Synthesis of materials

1.2.1. Synthesis of monomer 3,4-bis(but-3-en-1-yloxy)thiophene (Th-BE).

3,4-dimethoxythiophene (1) (1.44 g, 10 mmol), but-3-en-1-ol (2) (2,161 g, 30 mmol) and p-toluenesulfonic acid (0.19 g, 1.0 mmol) were charged into 250 mL of dry toluene and placed under reflux. The refluxing mixture was strongly flushed with argon every 2-4 hours, hence evacuating the generated methanol and displacing the equilibrium to the formation of Th-BE. This process was controlled by TLC and repeated until completion of the reaction. The dark yellow organic phase was washed with water and dried over anhydrous magnesium sulfate. Toluene was removed by rotary evaporation and the resulting dark oil was purified by column chromatography on silica with petroleum ether and dichloromethane as eluent (PE:DCM=5:1). The solvent was evaporated and Th-BE was obtained as a clear oil (yield: 60 %). ^1H NMR (400 MHz, Chloroform- d): δ 6.19 (s, 2H), 5.89 (ddt, $J = 17.0, 10.1, 6.8$ Hz, 2H), 5.20 - 5.07 (m, 4H), 4.03 (t, $J = 7.0$ Hz, 4H), 2.57 (q, $J = 6.8$ Hz, 4H). ^{13}C NMR (101 MHz, Chloroform- d): δ 146.25, 133.16, 116.07, 96.57, 68.68, 32.47.

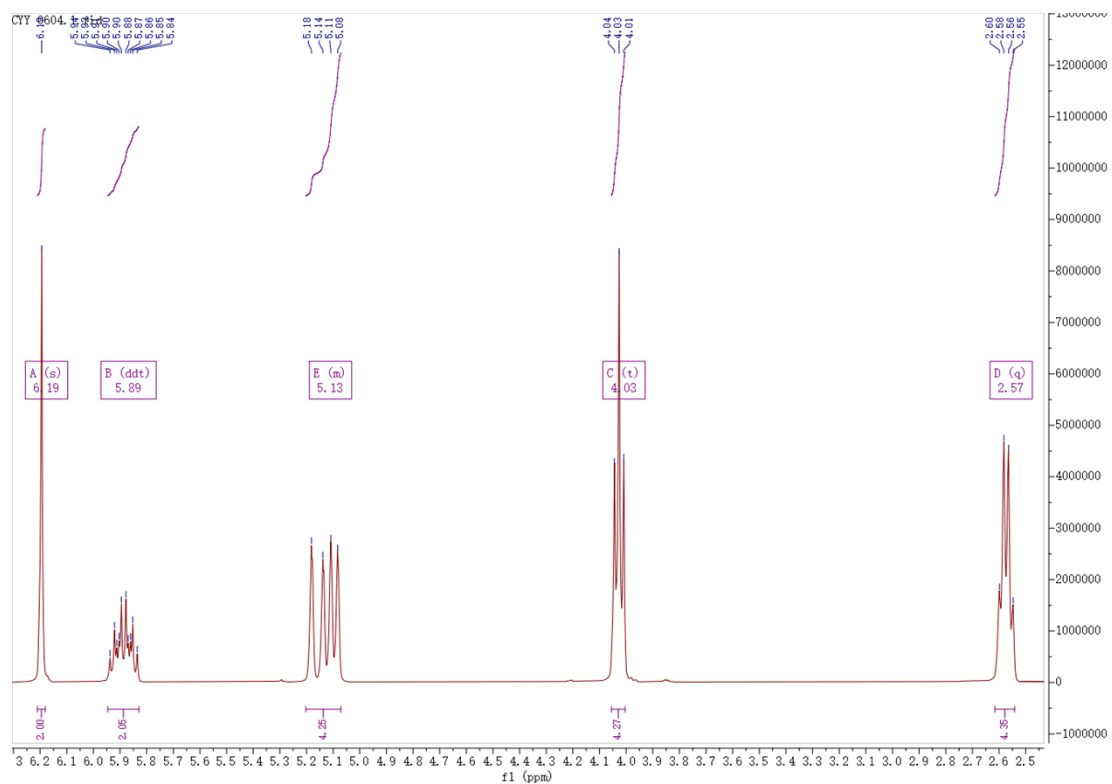


Figure S1. ¹H NMR of TH-BE.

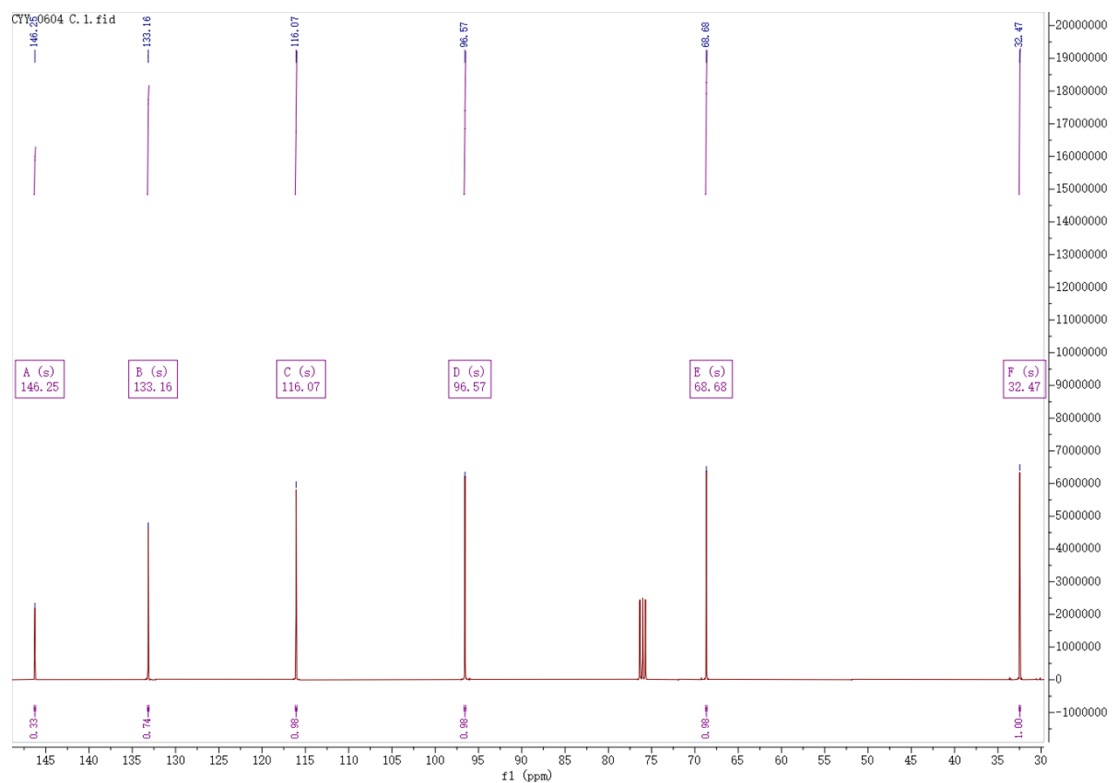


Figure S2. ¹³C NMR of TH-BE.

1.2.2. Synthesis of S@Th-BE

Three S@Th-BE composites with varying sulfur contents (25 %, 30 %, and 40 %) were synthesized through an inverse vulcanization process. The mass ratios of Th-BE: S₈: Ketjen Black (KB) were 2.5:2.5:5, 2:3:5, and 1:4:5, respectively. Taking 25 % S@Th-BE as an example, 25 mg of sulfur (S₈) and 25 mg of Th-BE were accurately weighed to achieve a 2.5:2.5 mass ratio. Each component was separately dissolved in carbon disulfide (CS₂) and ethanol to ensure uniform dispersion. The sulfur solution was gradually added to the Th-BE solution under continuous stirring to promote homogeneous mixing. In parallel, 50 mg of KB was dispersed in ethanol and subsequently introduced into the mixture. The combined solution was then dried in a vacuum oven at 40 °C, yielding a dry powder. This powder was finely ground using an agate mortar and transferred into a sealed reaction vessel inside a nitrogen-filled glove box. The inverse vulcanization reaction was conducted under an N₂ atmosphere by heating the mixture to 170 °C at a controlled rate of 4.7 °C/s and maintaining this temperature for 12 hours. After cooling to room temperature, the final composite, denoted as 25 % S@Th-BE, was collected for further characterization.

1.3. Preparation of electrolyte

The electrolyte formulation used in this paper was prepared following the protocol described in the referenced literature (*Small* 2023, 2207133), which was composed of 2 M (mol L⁻¹) zinc trifluoromethanesulfonate (Zn(CF₃SO₃)₂) and 50 mM (mmol L⁻¹) zinc iodide (ZnI₂), with deionized water and ethylene glycol

(EG) serving as co-solvents in a 1:1 volume ratio. The preparation involved the following steps: 3.6355 g of $\text{Zn}(\text{CF}_3\text{SO}_3)_2$ and 0.0798 g of ZnI_2 were weighed and combined. Subsequently, 2.5 mL of both deionized water and EG were pipetted into the mixture to achieve dissolution. The solution was then transferred to an oven overnight, resulting in a yellow mixed solution.

1.4. Assembly measurements of the zinc-sulfur battery

The S@Th-BE cathode was prepared using a S@Th-BE composite: Ketjen Black (KB): PTFE binder in a mass ratio of 8:1:1. The fabrication process began by thoroughly mixing S@Th-BE and KB in ethanol, followed by grinding to ensure uniform dispersion. PTFE was then introduced into the mixture, and further grinding was performed until a stretchable sheet was formed. This cathode sheet was then transferred onto a pre-cleaned titanium mesh current collector, which had been previously washed with ethanol. The sheet was compressed into a thin film using a rolling machine, achieving an average active material loading of 1.0-2.0 mg cm^{-2} . The electrode films were dried under vacuum at 40 °C for 12 hours, then cut into appropriate sizes. After drying, the films were weighed, the active material loading was typically maintained within the range of 1.0-2.0 $\text{mg}_{(\text{sulfur})}$. The assembled zinc-sulfur battery was configured as a CR2032-type coin cell, with pure metallic zinc as the anode and glass fiber (GF/D) as the separator. Each cell was filled with 100 μL of the above-prepared electrolyte.

1.5. Materials characterizations

X-ray diffraction (XRD, Empyrean, Panalytical B.V., Almelo, Netherlands) was

employed to analyze S@Th-BE using Cu K α radiation, with a scanning range of 5° to 80° (40 kV, 40 mA, scanning rate of 5° min⁻¹). The ex-situ XRD measurements were conducted on nearly ten different cathode states at various charge/discharge stages at 3th cycle. Long-cycle XRD measurements were conducted on scratched cathode powders collected after 100 cycles, in both charged (1.6 V) and discharged (0.05 V) states. The X-ray photoelectron spectroscopy (XPS, ESCALAB 250 Xi, Thermo Scientific Escalab, USA) was used to analyze the valence states of carbon (C), sulfur (S). Ex-situ XPS was conducted on samples in three different electrochemical states: as-prepared, fully charged (1.6 V), and fully discharged (0.05 V). Transmission electron microscopy (TEM, Talos 200S, Thermo Fisher Scientific (FEI), USA), combined with elemental mapping, was used to observe the morphology and structural evolution of the composite material after cycling. Thermogravimetric analysis (TG, TGA2, METTLER TOLEDO, Switzerland) was conducted under a nitrogen atmosphere within a temperature range of 30-1100°C at a heating rate of 10°C min⁻¹. Fourier-transform infrared spectroscopy (FTIR, Nicolet iS50, Thermo Scientific Escalab, USA) was utilized to identify functional groups and bond variations in unknown substances, with a scanning range of 4000-100 cm⁻¹. Raman spectroscopy (Raman, LabRAM HR Evolution, HORIBA Jobin Yvon S.A.S., France) was employed to investigate molecular structures and chemical bond changes, with a scanning range of 100-4000 cm.

1.6. Electrochemical tests

Galvanostatic charge/discharge cycling was conducted on a battery instrument (Land CT3002A test system, Wuhan LAND Electronic Co. Ltd., Wuhan, China) within a cutoff voltage window of 0.05-1.60 V (vs Zn/Zn²⁺), with the specific capacity calculated based on the mass of sulfur. Cyclic voltammetry (CV) was also conducted on the same workstation, with a potential range of 0.05 to 1.60 V and a scan rate of 0.1 mV s⁻¹. Before all electrochemical performance tests, the battery was left to stand for 12 hours to allow the electrolyte to fully infiltrate the anode and cathode. The electrochemical tests for the three S@Th-BE cathodes with different sulfur contents were conducted under the same conditions described above.

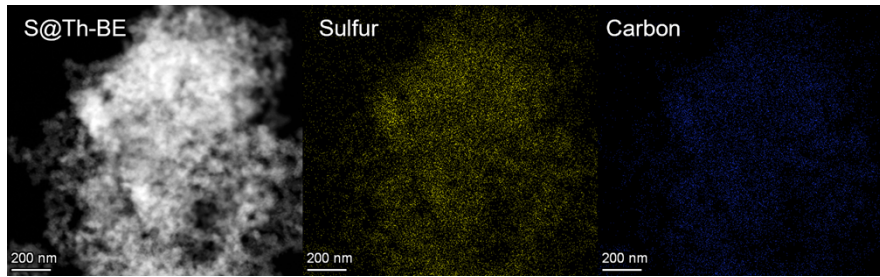


Figure S3. EDS elemental mapping images of the S@Th-BE composite, showing the uniform distribution of sulfur and carbon across the structure.

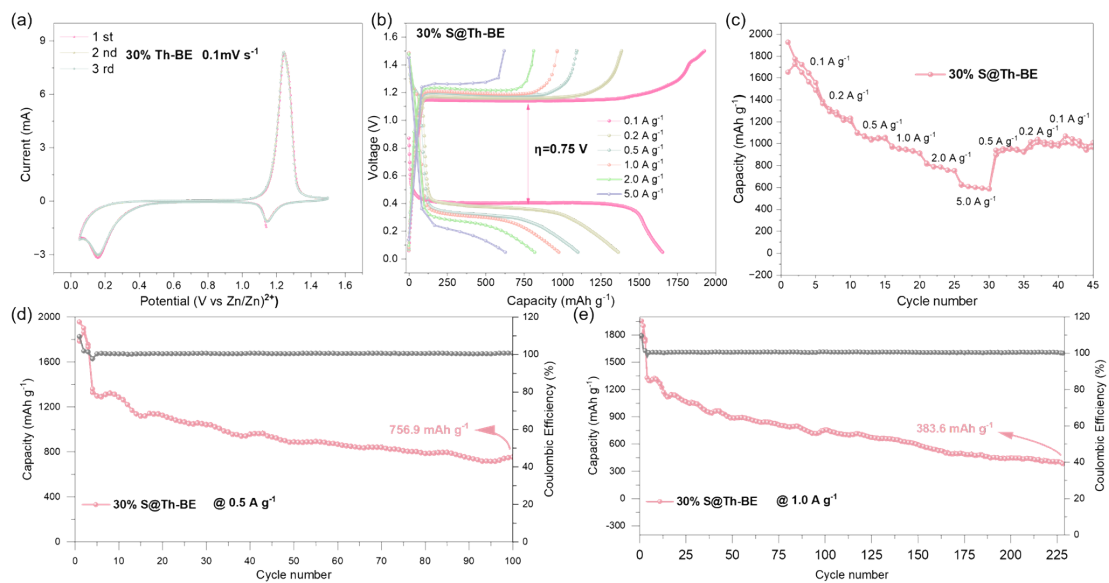


Figure S4. Electrochemical performance of the 30 % S@Th-BE cathode. (a) Cyclic voltammetry (CV) curves at 0.1 mV s^{-1} . (b) Galvanostatic charge-discharge profiles at different current densities. (c) Rate performance comparison between S@Th-BE and S@KB. (d)-(e) Long-term cycling performance at 0.5 A g^{-1} and 1.0 A g^{-1} .

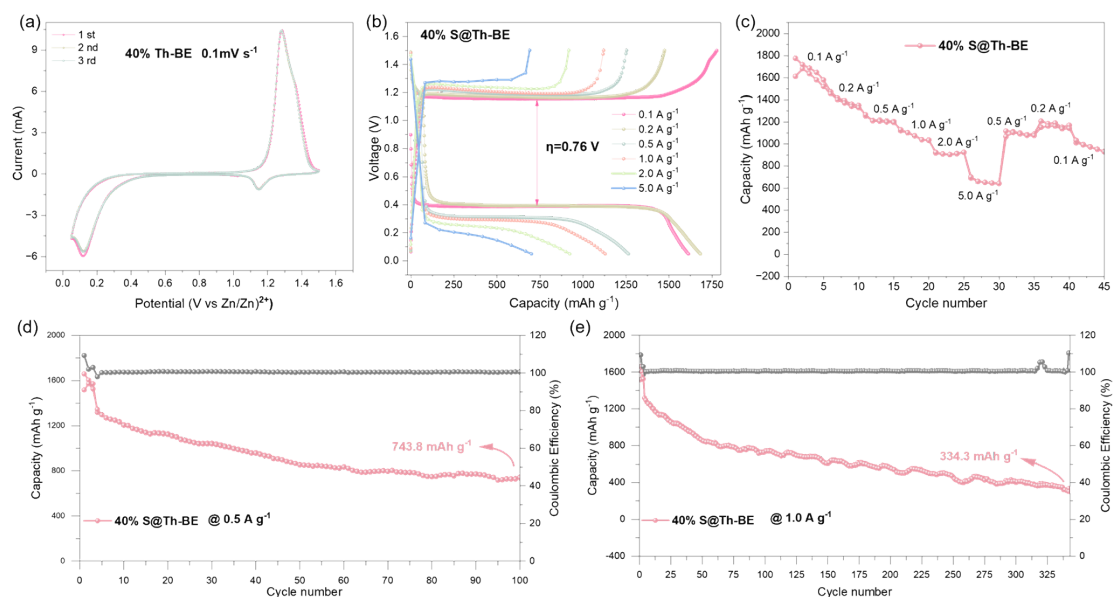


Figure S5. Electrochemical performance of the 40 % S@Th-BE cathode. (a) Cyclic voltammetry (CV) curves at 0.1 mV s^{-1} . (b) Galvanostatic charge-discharge profiles at different current densities. (c) Rate performance comparison between S@Th-BE and S@KB. (d-e) Long-term cycling performance at 0.5 A g^{-1} and 1.0 A g^{-1} .

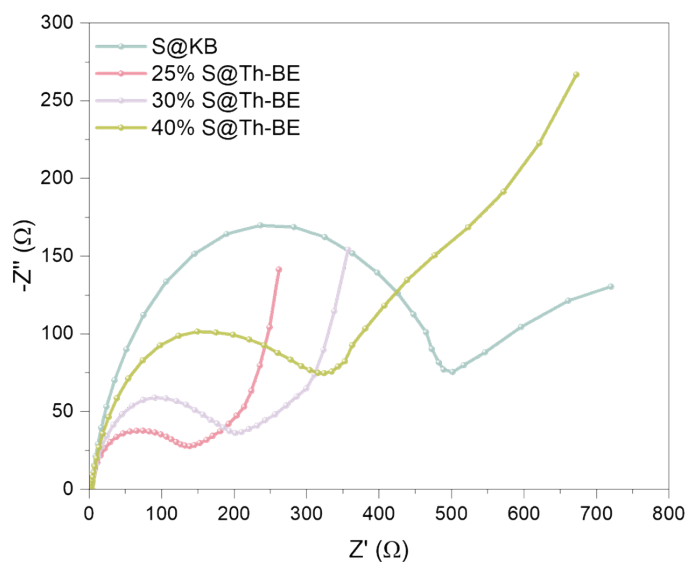


Figure S6. Electrochemical impedance spectroscopy (EIS) curves of Zn-S batteries with different sulfur contents measured at the initial state. As the sulfur content increases, the semicircle diameter becomes larger, indicating an increase in charge transfer resistance. Notably, the sample without Th-BE exhibits the largest resistance, confirming that the introduction of the Th-BE framework facilitates enhanced reaction kinetics and improves electrode conductivity.

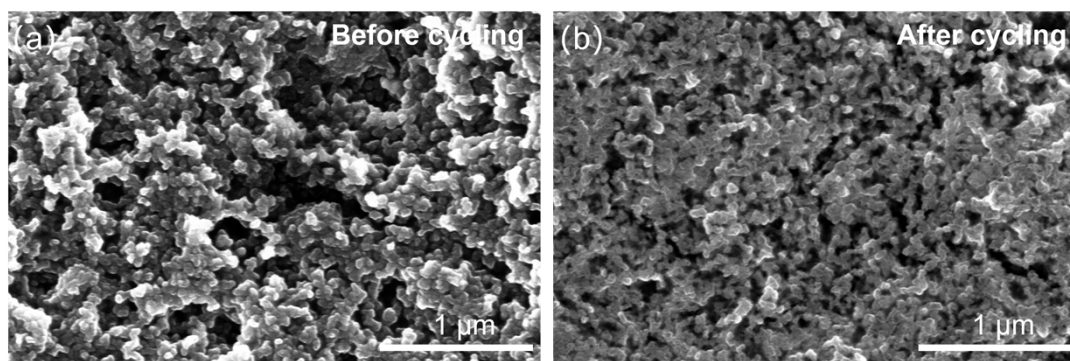


Figure S7. SEM images of the S@Th-BE electrode (a) before cycling and (b) after 100 charge-discharge cycles. The electrode retains a compact and continuous morphology with no apparent structural collapse, confirming the stabilizing effect of the Th-BE framework on long-term cycling.

3. Supplementary table

Table S1. Comparison of the electrochemical performance with other reported Zn-S batteries.

Cathode material	Cathode active material loading(mg/cm ²)	Electrolyte	Voltage windows (V)	Specific capacity(mAh g ⁻¹ /A g ⁻¹)	Capacity(mAh g ⁻¹) after cycling, cycles, current density	Ref.
S@CNTs-50 (S@CNTs-50:AB:PTFE=8:1:1)	3-5	1 M ZnAc ₂ + 0.05 wt% I ₂	0.05-1.6	1105.0/0.1	450, 225, 2 A g ⁻¹	[1]
ZnS@CF (ZnS@CF:KB:PTFE=8:1:1)	1.5-3	3 M ZnSO ₄ + 1 wt% TUI	0.1-1.4	465/0.1	226, 300, 2 A g ⁻¹	[2]
FeNC/NC/CC	2.0-2.6	2 M ZnSO ₄	0.1-1.6	1143/0.2	519, 300, 0.5 A g ⁻¹	[3]
ZnS _{1-x} Se _x	2.5	2 M ZnSO ₄ + 50 mM ZnI	0.2-1.7	1518.6/0.1	504.4, 200, 2 A g ⁻¹	[4]
PAC/S-60.33% (PAC/S-60.33%:Super P:Guar gum=7:1.5:1.5)	1.4-1.8	2 M Zn(OTF) ₂ + 0.15 wt% I ₂	0.1-1.6	633.5/0.5	180, 400, 5 A g ⁻¹	[5]
KB-S (KB-S:KB:Sodium alginate=7:2:1)	3.9-8.3	1 M ZnCl ₂	0.1-1.5	1668.0/0.01	75, 100, /	[6]
CMK-3@S (CMK-3@S:AB:PVDF=8:1:1)	1-2	3 M Zn(OTF) ₂ + 0.1 wt% I ₂	0.05-1.75	1174.0/0.2	450, 200, 1 A g ⁻¹	[7]

KB/S (KB/S:guargum:Super P=8:1:1)	1.4-1.6	3 M ZnSO ₄ + 0.05 m ZnI ₂	0.15-1.4	1580.0/0.5	100, 550, 5 A g ⁻¹	[8]
S@NPC (S@NPC:super-P:PTFE=8:1:1)	3	2 M Zn(OTF) ₂ + 50 mM ZnI ₂	0.05-1.6	1435/0.1	300, 250, 3 A g ⁻¹	[9]
S/CSs (S/CSs:AB:PVDF=8:1:1)	2	8 M Zn(ClO ₄) ₂	0.05-2.1	1284/0.1	169, 500, 2 A g ⁻¹	[10]
S@AC3000 (S@AC3000:KB:PTFE=6:3:1)	1	1 M Zn(CH ₃ COO) ₂ + 1M LiTFSI	0.25-1.55	699.3/1	450, 384, 2.5 A g ⁻¹	[11]
S@Th-BE (S@Th-BE:KB:PTFE=8:1:1)	1-2	3 M Zn(OTF) ₂ + 50 mM ZnI ₂ + EG	0.05-1.5	1773.9/0.1	379.6, 310, 1 A g ⁻¹	This work

AB: acetylene black; KB: ketjen black; PTFE: polytetrafluoroethylene binder; TUI: iodinated thiourea; PVDF: polyvinylidene fluoride; EG: ethylene glycol; Ac:CH₃COO⁻;

Supplementary references

- [1] Li, W.; Wang, K.; Jiang, K. A Low Cost Aqueous Zn–S Battery Realizing Ultrahigh Energy Density. *Advanced Science* **2020**, *7* (23). DOI: 10.1002/adv.202000761.
- [2] Liu, D.; He, B.; Zhong, Y.; Chen, J.; Yuan, L.; Li, Z.; Huang, Y. A durable ZnS cathode for aqueous Zn-S batteries. *Nano Energy* **2022**, *101*. DOI: 10.1016/j.nanoen.2022.107474.
- [3] Zhang, W.; Wang, M.; Ma, J.; Zhang, H.; Fu, L.; Song, B.; Lu, S.; Lu, K. Bidirectional Atomic Iron Catalysis of Sulfur Redox Conversion in High - Energy Flexible Zn–S Battery. *Advanced Functional Materials* **2023**, *33* (11). DOI: 10.1002/adfm.202210899.
- [4] Ren, Y.; Li, J.; Zhang, Y.; Huang, Y.; Li, Z. Trace Selenium Doping for Improving the Reaction Kinetics of ZnS Cathode for Aqueous Zn–S Batteries. *Small* **2024**. DOI: 10.1002/smll.202402466.
- [5] Wang, K.; Wang, J.; Zhang, Z.; Zhang, W.; Fu, F.; Du, Y. Pitch-derived 3D amorphous carbon encapsulated sulfur-rich cathode for aqueous Zn-S batteries. *Science China Chemistry* **2023**, *66* (9), 2711-2718. DOI: 10.1007/s11426-023-1711-x.
- [6] Luo, L.-W.; Zhang, C.; Wu, X.; Han, C.; Xu, Y.; Ji, X.; Jiang, J.-X. A Zn–S aqueous primary battery with high energy and flat discharge plateau. *Chemical Communications* **2021**, *57* (77), 9918-9921. DOI: 10.1039/d1cc04337d.
- [7] Xu, Z.; Zhang, Y.; Gou, W.; Liu, M.; Sun, Y.; Han, X.; Sun, W.; Li, C. The key role of concentrated Zn(OTf)₂ electrolyte in the performance of aqueous Zn–S batteries. *Chemical Communications* **2022**, *58* (58), 8145-8148. DOI: 10.1039/d2cc02075k.
- [8] Hei, P.; Sai, Y.; Liu, C.; Li, W.; Wang, J.; Sun, X.; Song, Y.; Liu, X. X. Facilitating the Electrochemical Oxidation of ZnS through Iodide Catalysis for Aqueous Zinc - Sulfur Batteries. *Angewandte Chemie International Edition* **2024**, *63* (9). DOI: 10.1002/anie.202316082.
- [9] Guo, Y.; Chua, R.; Chen, Y.; Cai, Y.; Tang, E. J. J.; Lim, J. J. N.; Tran, T. H.; Verma, V.; Wong, M. W.; Srinivasan, M. Hybrid Electrolyte Design for High - Performance Zinc – Sulfur Battery. *Small* **2023**, *19* (29). DOI: 10.1002/smll.202207133.
- [10] Chen, Z.; Huang, Z.; Zhu, J.; Li, D.; Chen, A.; Wei, Z.; Wang, Y.; Li, N.; Zhi, C. Highly Reversible Positive - Valence Conversion of Sulfur Chemistry for High - Voltage Zinc – Sulfur Batteries. *Advanced Materials* **2024**, *36* (30). DOI: 10.1002/adma.202402898.
- [11] Wang, L.; Xu, Y.; Xiao, L.; Liu, Y.; Wang, L.; Zha, S.; Zhang, S.; Jin, J. Ionic Covalent Organic Framework Membrane as Active Separator for Highly Reversible Zinc–Sulfur Battery. *ACS Applied Materials & Interfaces* **2024**, *16* (38), 50036-50044. DOI: 10.1021/acsami.4c11422.